Redox Biology 46 (2021) 102068

Contents lists available at ScienceDirect

Redox Biology

journal homepage: www.elsevier.com/locate/redox

A novel fluorescent probe for the detection of peroxynitrite and its application in acute liver injury model

Chen Jin [a,1], Pengfei Wu [b,c,1], Yushun Yang [a], Zhenxiang He [a,***], Hailiang Zhu [a,**], Zhen Li [a,*]

[a] State Key Laboratory of Pharmaceutical Biotechnology, School of Life Sciences, Nanjing University, No.163 Xianlin Road, Nanjing, 210023, China
[b] Pancreas Center, The First Affiliated Hospital of Nanjing Medical University, Jiangsu Province Hospital, Nanjing, 210029, China
[c] Pancreas Institute of Nanjing Medical University, Nanjing, 210029, China

ARTICLE INFO

Keywords:
Acute liver injury
Fluorescent probe
Peroxynitrite detection
In vivo imaging

ABSTRACT

Realizing the early diagnosis of acute liver injury has become a hotspot in recent years. Since the current indexes are not specific, developing novel probes with new recognition group remains a necessity. In this work, we developed a novel fluorescent probe, **NNP**, for the detection of $ONOO^-$ in acute liver injury (ALI). The *in vitro* evaluation of **NNP** indicated the advantages including high sensitivity (LOD = 0.13 μM), rapid response (<25 s), naked-eye (red to yellow), and stability under various pH (4–10) and time (>48 h) conditions. Accordingly, **NNP** achieved the dose-dependent detection of $ONOO^-$ in human hepatic stellate LX-2 cells. Further, in the ALI model mice, **NNP** could monitor the $ONOO^-$ level in the occurrence of ALI in situ (in the liver region) with a steady performance. Subsequent immunohistochemical and imaging studies confirmed that **NNP** could achieve the detection of endogenous $ONOO^-$ in ALI liver tissues. This work introduced a practical implement for the $ONOO^-$ detection in ALI as well as a referable example for the establishment of molecular indexes in pre-clinical diagnosis.

1. Introduction

In all medicinal and therapeutic theories, liver acts as one of the five major organs in human body, and participates deeply in the procedure of metabolism [1,2]. Since the pace of modern life increases, the liver is also facing the threat of damage induced by ethanol, drugs and toxic materials [3–5]. Consequently, acute injury occurred more frequently in liver tissues. As a typical clinical symptom, acute liver injury (ALI) usually exhibited a dramatic failure of hepatocyte function with no previously disease-suffering in liver [6,7]. Actually, with the accurate early assessment, ALI is reversible under rational treatment or even simply getting rid of the injury sources. Therefore the challenging problem is how to realize the early diagnosis of ALI, which has become a hotspot in recent years [8,9].

For ALI, common clinical index of diagnosis includes alanine aminotransferase (ALT) [10], aspartate aminotransferase (AST) [11], alkaline phosphatase (ALP) [12], and γ-glutamyltranspeptidase (GGT) [13]. It is a pity that the blood tests based on the evaluation of these enzymes can be affected by various other diseases, that is, the tests are not specific [14,15]. Moreover, these manifestations are all post-symptom, which cannot fulfill the real-time detection in the physiological and pathological events with constant fluctuations. On the contrary, optical probes are practical implements for the above mentioned requirements with advantages including high sensitivity, high resolution, as well as noninvasive and rapid imaging [16,17]. Accompanied with good permeability and biocompatibility, they can achieve the real-time and in situ monitoring. Specifically for ALI, potential biomarkers which can be detected by optical probes include reactive nitrogen species (eg. $ONOO^-$) [18,19], reactive sulfur species (H_2S and H_2S_n) [19], enzymes (LAP, MAO, and ALP) [20–22]. Among them, peroxynitrite ($ONOO^-$) seems the most frequently associated one. It is a stronger oxidant than hydrogen peroxide, and consists of a superoxide anion and nitric oxide combination with a short half-life (~10 ms) [23,24]. Although peroxynitrite also inferred correlation with a variety of diseases [25,26], by in situ monitoring, it could be closely related to ALI. Till now, many $ONOO^-$ probes have been designed with

* Corresponding author.
** Corresponding author.
*** Corresponding author.
E-mail addresses: zxhe@nju.edu.cn (Z. He), zhuhl@nju.edu.cn (H. Zhu), lizhenzfx@nju.edu.cn (Z. Li).
[1] These authors contributed equally to this work.

https://doi.org/10.1016/j.redox.2021.102068
Received 30 May 2021; Accepted 8 July 2021
Available online 10 July 2021

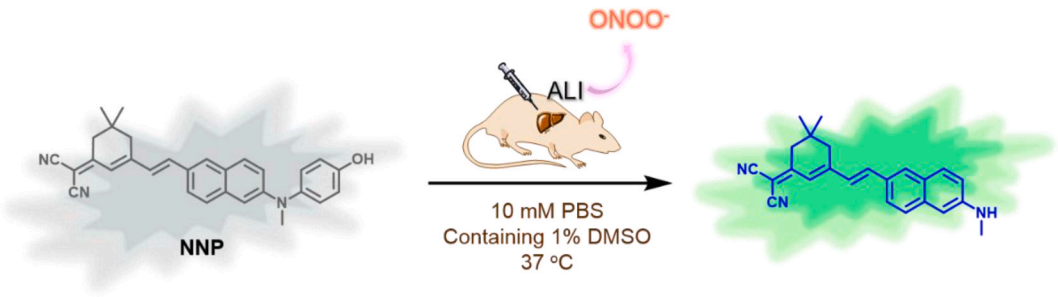

Fig. 1. The illustration of the probe **NNP** for the detection of peroxynitrite.

the recognition moieties including borate ester [27–31], isatin [32], rhodamine [33], xanthene [34–36], diphenylphosphine ester [37,38] and nitrobenzoate [39]. However, an ideal probe for $ONOO^-$ should contain the reaction mechanism which is more specific than redox. Accordingly, developing novel probes with new recognition group remains a necessity [40].

In this work, we exploited a novel fluorescent probe, **NNP**, for the detection of $ONOO^-$ with a newly involved sensing group (Fig. 1). After the evaluation of optical properties *in vitro*, **NNP** was applied in the ALI mice model. We expect that this novel implement for liver injury detection could excite more inspiration on this topic, and help the medical researches as well as clinical trials.

2. Experimental section

2.1. Material and methods

All reagents used for synthesis were obtained from Aladdin without further purification. Column chromatography was performed on silica gel (200–300 mesh). ^1H and ^{13}C NMR spectra were recorded in $CDCl_3$, DMSO-d_6 at room temperature on Bruker DRX-600 (600 MHz). Mass spectra were obtained at the Mass Spectrometry Facility at Nanjing University. Fluorescence studies were carried out with F-7000 Fluorescence Spectrophotometer. UV spectrum was treated in UV-2550 ultraviolet spectrophotometer. Ordinary section was imaging on microscope (Olympus IX73). Confocal fluorescence images were recorded on TCS SP8 MP two-photon confocal fluorescent microscope (Leica). In vivo imaging was carried out on PE IVIS Lumina XR III. All pH measurements were carried out on pH meter of PHS-25. The flow cytometer model was CytoFlex.

The stock solution of the probe **NNP** was diluted at 1 mM in DMSO for further testing. Other testing analytes were prepared from the H_2O_2, NaClO, Cysteine, Glutathione, Homocysteine, CH_3COONa, NaCl, Na_2CO_3, $NaNO_2$, $NaNO_3$, Na_2SO_3, Na_2S, $CaCl_2$, $MgCl_2$, $FeSO_4$, $AlCl_3$, $CuCl_2$ in the doubly distilled water. The reactive oxygen species (ROS) were prepared following the methods of reported literature [41]. Ultrapure water was produced from a Milli-Q reference system (Millipore Elix 5). Slight changes in pH variations of the PBS buffer were achieved by adding the minimum volumes of HCl or NaOH (1 M). All spectroscopic measurements of the probe **NNP** (10 μM) were performed in pH 7.4, 10 mM phosphate buffer with 1% DMSO and 2 mM CTAB. All the spectroscopic reactions were tested at 37 °C. Unless otherwise noted, for all the measurements, the excitation wavelength was 432 nm, the both excitation and emission slit widths were 10 nm and the voltage was 600 V. The emission spectrum was measured and scanned from 450 nm to 650 nm at 1200 nm/min.

2.2. Synthesis of the compounds

2.2.1. 6-((4-methoxyphenyl)(methyl)amino)-2-naphthaldehyde (compound **3**)

A solution of Cs_2CO_3 (815 mg, 2.5 mmol), $Pd(OAc)_2$ (18 mg, 0.08 mmol), and BINAP (87 mg, 0.14 mmol) were added in 20 mL dry toluene was stirring at 110 °C for 10 min under N_2 protection. Then the compound **1** (235 mg, 1 mmol) and compound **2** (137 mg, 1 mmol) were added immediately. The mixed contain all the ingredients was reacted another 18 h at 110 °C for 10 min under N_2 protection. After the reaction was over, the solids in the reaction solution were filtered out upon cooling to room temperature. After removal of the solvent under reduced pressure by evaporation, the crude product was purified by silica column chromatography using PE/EtOAc (v/v 80:1) as eluent, obtaining 195 mg light-yellow compound **3** (Yield 67%). ^1H NMR (600 MHz, DMSO) δ 9.98 (s, 1H), 8.31 (s, 1H), 7.85 (d, J = 9.1 Hz, 1H), 7.80–7.68 (m, 2H), 7.27–7.17 (m, 2H), 7.11 (d, J = 2.3 Hz, 1H), 7.06–6.90 (m, 3H), 3.79 (s, 3H), 3.35–3.28 (m, 3H). ^{13}C NMR (151 MHz, DMSO) δ 192.46, 157.54, 150.17, 140.70, 138.60, 135.02, 131.04, 130.73, 128.07, 127.33, 125.94, 123.41, 118.80, 115.62, 107.25, 55.75, 41.02.

2.2.2. (E)-2-(3-(2-(6-((4-methoxyphenyl)(methyl)amino)naphthalen-2-yl)vinyl)-5,5-dimethylcyclohex-2-en-1-ylidene)malononitrile (compound **5**)

A solution of compound **3** (170 mmg, 0.6 mmol) and compound **4** (167 mg, 0.9 mmol, the synthesis scheme referring to the literature of our group [42]) were added in 10 mL dry ethyl alcohol was stirring at 80 °C for 2 min. Then the mixture was dripped into piperidine and reflux for 12 h. After the reaction was over, the solid was separated upon cooling to room temperature to obtain 136 mg dark red compound **5** without further purification (Yield 48%). ^1H NMR (600 MHz, DMSO) δ 7.96 (s, 1H), 7.78 (d, J = 7.7 Hz, 1H), 7.66 (dd, J = 17.5, 8.6 Hz, 2H), 7.42 (d, J = 14.4 Hz, 2H), 7.19 (d, J = 7.0 Hz, 2H), 7.13–6.84 (m, 5H), 3.78 (s, 3H), 2.60 (d, J = 21.9 Hz, 4H), 1.03 (s, 6H). ^{13}C NMR (151 MHz, DMSO) δ 192.45, 192.42, 157.54, 150.17, 140.69, 138.58, 134.99, 131.02, 130.70, 128.06, 128.03, 127.31, 125.92, 123.38, 118.78, 115.61, 115.57, 115.48, 107.23, 107.19, 56.50, 55.74, 41.02, 18.99.

2.2.3(E)-2-(3-(2-(6-((4-hydroxyphenyl)(methyl)amino)naphthalen-2-yl)vinyl)-5,5-dimethylcyclohex-2-en-1-ylidene)malononitrile (NNP)

Dissolve the compound **5** (95 mg, 0.21 mmol) into 15 mL dry DCM under ice bath conditions. Then BBr_3 (525 mg, 200 μL, 1.05 mmol) was added drop by drop and stirred at 0 °C for 1 h. The mixture was kept reacting at room temperature for 12 h. After quenched by saturated $NaHCO_3$, the solution was extracted by DCM and dried with anhydrous Na_2SO_4. After removal of the solvent under reduced pressure by evaporation, the crude product was purified by silica column chromatography using PE/EtOAc (v/v 6:1) as eluent, obtaining 66.7 mg black solid (**NNP**, Yield 70%). ^1H NMR (600 MHz, DMSO-d6) δ 9.50 (s, 1H), 7.94 (d, J = 1.7 Hz, 1H), 7.76 (dd, J = 8.7, 1.8 Hz, 1H), 7.63 (dd, J = 17.9, 8.9 Hz, 2H), 7.45–7.33 (m, 2H), 7.07 (d, J = 8.6 Hz, 2H), 7.01 (d, J = 2.5 Hz, 1H), 6.93 (dd, J = 9.0, 2.5 Hz, 1H), 6.87–6.81 (m, 3H), 3.29 (s, 3H), 2.59 (s, 2H), 2.55 (s, 2H), 1.02 (s, 6H). ^{13}C NMR (151 MHz, DMSO) δ 169.53, 155.81, 154.52, 147.82, 138.62, 137.93, 134.82, 129.22, 128.51, 128.39, 127.09, 126.88, 126.09, 125.84, 123.85, 121.27, 117.62, 115.72, 113.53, 112.70, 106.37, 74.40, 41.65, 31.05, 26.84.

2.3. Determination of the fluorescence quantum yield

Fluorescence quantum yield (FQY) was determined using aqueous solution of Rhodamine B as a standard ($\Phi = 0.69$, 10 μM in ethyl alcohol, λ_{ex} = 365 nm). By measuring absorption and fluorescence spectra of **NNP** according to equation, calculated and finally get the quantum yield. The quantum yield Φ as a function solvent polarity is calculated using equation as follows:

$$\Phi_u = [(A_s F_u n_u^2)/(A_u F_s n_s^2)]\Phi_s$$

Where Φ_s is the quantum yield, Fs and Fu is the areas' integral values of the corrected fluorescence spectra of the reference and testing solution, A_s and A_u stand for the absorbance of the reference and testing solution, n_u and n_s are the solvent refractive indexes of sample and reference, respectively.

Quantum yield: $\Phi = 0.27$.

2.4. The limit of detection (LOD) of ***NNP***

The emission spectrum of free **NNP** in PBS buffer (10 mM, pH = 7.40, CTAB 2 mM, containing 1% DMSO) was collected for 30 times to confirm the background noise σ. The linear regression curve was then fitted according to the data in the range of $ONOO^-$ from 0 to 10 μM and obtained the slope of the curve. The detection limit (3σ/slope) was then determined to be 0.13 μM, which facilitate the quantitative detection of $ONOO^-$ in complex living body environment.

2.5. Cell culture, flow cytometry assays and imaging

LX-2 cells were cultured in Dulbecco's Modified Eagle Medium media (DMEM, Gibco) supplemented with 10% special grade fetal bovine serum (FBS, Gibco) and 1% antibiotics (100 U/mL penicillin and 100 μg/mL streptomycin, Vicente) at 37 °C and 5% CO_2. The LX-2 cells were seeded in the 6-well plates at the density of 1×10^5 cells per well. After adherent, the cells were cultured for 0.5 h with **NNP** (10 μM). After washing three times with DPBS, the cells were digested with trypsin (without EDTA), beaten evenly with 500 mL DPBS and added into the flow tube. Then added different concentrations of $ONOO^-$ (0–50 μM) for 0.5 h. The procedures were treated in accordance with the manufacturer's protocol, and the data were processed using Flow Jo software.

Before the imaging experiments, 1 mL of LX-2 cells were subcultured and seeded in the glass bottom culture dishes (Corning) at a density of 1×10^5 cells per well. After adherent, the cells were cultured for 0.5 h with **NNP** (10 μM). After washing with PBS buffer to wipe out the residual probe in the surface, the LX-2 cell were further incubated with different concentrations of $ONOO^-$ (0–50 μM) for 0.5 h at 37 °C. The cells were imaged respectively by two-photon confocal microscope. For monitoring the endogenous $ONOO^-$, the cells were pretreated with or without NAC (1×10^{-3} M, 12 h), FeTMpyp (100×10^{-6} M, 0.5 h), SIN-1 (200×10^{-6} M, 0.5 h), LPS (0.1 μg mL−1, 12 h), PMA (100×10^{-6} M, 1 h) and the cells were pretreated with 1 mM CCl_4 for 4 h at 37 °C, then incubated with **NNP** (10 μM) for another 0.5 h and imaged after washing with PBS three times. The cell imaging detected by a Lecia Two-photon fluorescence microscope equipped with 40× objective lens. The excited wavelength was set at 405 nm, and emission wavelengths were collected from 530 nm to 600 nm.

2.6. Cytotoxicity assay

Cell cytotoxicity was assessed with a standard CCK-8 method. LX-2 cells were seeded into 96-well plates, the diluted cell suspension (5×10^3 per well) 100 μL was added to each well of 96-well culture plates. After adherent overnight, several concentrations of **NNP** (0, 5, 10, 15, 20, 25, 30, 35, 40 μM) were added. After 24 h exposure period, the culture solution was replaced with 10 μL of CCK-8 reagent for each well, and the cell samples were further incubated for 1 h. The mixture solution was measured with an ELISA reader (ELx800, BioTek, USA) at 450 nm. In all experiments, 10 replication wells were used for each probe concentration. The experiments were repeated six times.

2.7. Establishment of animal models

BAIB/c Nude mice were purchased from Institute of Zoology, Nanjing University. All animal care and experimental protocols complied with the Animal Management Rules of the Ministry of Health of the People's Republic of China and were approved by the Institute of Process Engineering, Chinese Academy of Sciences. The mice were divided into two groups. One group of mice used it directly without any other treatment as wide-type mice, and one group created model mice.

For CCl_4-induced ALI model mice, a mixture of CCl_4 (10 mL/kg bodyweight) and olive oil (1:9 (w/v)) was used to induce acute liver injury. Model group were i.p. injected with CCl_4 for 24 h. At the end of the experiment, mice were sacrificed after anesthetization with Isoflurane gas anesthesia. The abdominal cavity was then opened to separate the liver, and a camera was used to take pictures of the complete liver of the mouse. A small portion of the liver was removed and immobilized in 10% formalin solution for histopathological, immunohistochemical and imaging studies.

In acetaminophen (APAP)-induced hepatotoxicity model, the prepared APAP (20 mg/mL in normal saline (NS)) solution was used to induce hepatotoxicity model. Model group were i.p. injected with APAP solution (dosage of administration was 200 mg/kg, 400 mg/kg) for 1 h. The model of alcohol-induced liver injury was established by gavage of 50% alcohol (150 μL). At the end of the experiment, mice were sacrificed after anesthetization with Isoflurane gas anesthesia. The abdominal cavity was then opened to separate the liver, and immobilized in 10% formalin solution for imaging studies.

2.8. Detection of serum liver injury indexes

Both the control group and model group mice were selected, rapid extraction of blood from orbit with a capillary of 0.05 mm inner diameter. The collected serum samples were left standing at room temperature for 2 h, centrifuged at 3500 r/min for 15 min and collecting supernatant. The supernatant was re-centrifuged for 10 min at 3500 r/min.

Serum liver injury indexes were detected using the ALT, AKP, LDH, TBIL Detection Kit (YI FEI XUE BIO TECH). In addition, liver injury indexes were further confirmed by the Mice IV-C ELISA kit, Mice HYP ELISA kit (YI FEI XUE BIO TECH). All experiments were measured with an ELISA reader (ELx800, BioTek, USA), and set the parameters according to the kit instructions. The procedures were treated in accordance with the manufacturer's protocol.

2.9. In vivo imaging of mice

The mice were intraperitoneally injected with **NNP** 100 μM in saline (10 mL/kg) and imaging with small animal *in vivo* imaging system. After, the mice were intraperitoneally injected with $ONOO^-$ 400 μM (500 μL in saline). The fluorescent images of each group were measured at the different time interval within 5 min. The excited wavelength was set at 440 nm.

For all the CCl_4-induced model mice, 10% CCl_4 (in olive oil, 10 mL/kg) was intraperitoneally injected for 24 h. The wild type and model mice were intraperitoneally injected with **NNP** 100 μM in saline (10 mL/kg), respectively. Fluorescent images of mice were captured at different time interval within 1 h. The excited wavelength was set at 440 nm.

In acetaminophen (APAP)-induced hepatotoxicity model, Balb/c nude mice were administrated (i.p.) with 0 mg/kg, 200 mg/kg, 400 mg/kg APAP for 1.0 h. Babl/c nude mice were first administrated (i.p.) with

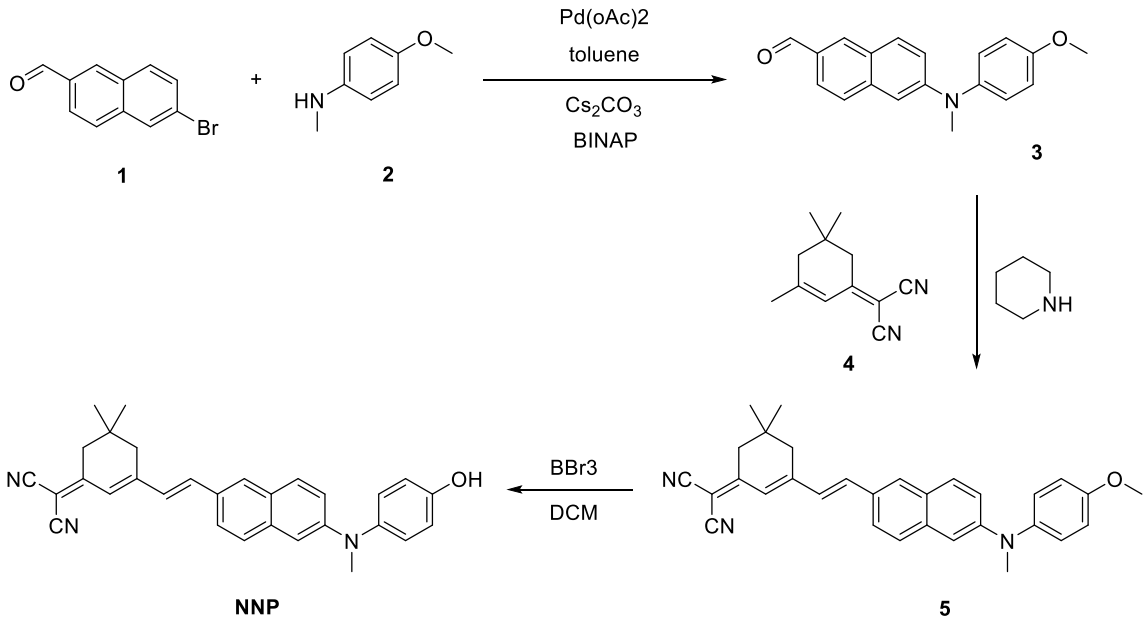

Fig. 2. The synthesis approach of the probe **NNP**.

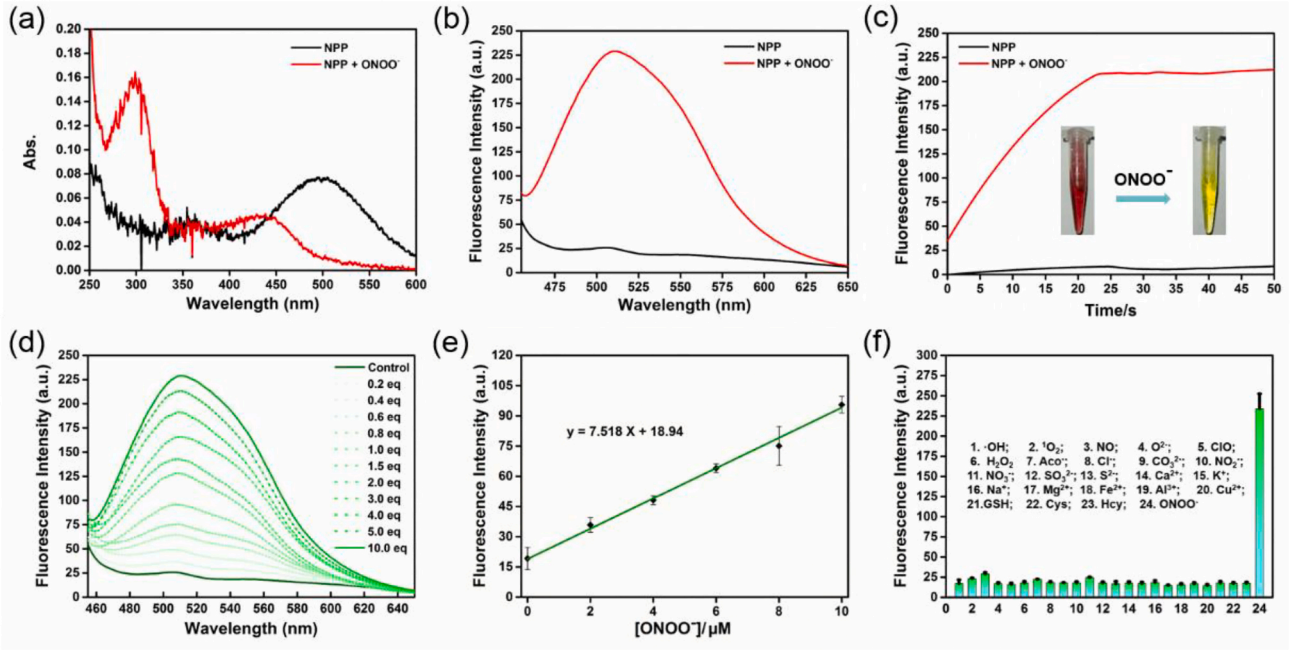

Fig. 3. (a) Absorption and (b) fluorescence of **NNP** (10 μM) in the absence and presence of $ONOO^-$ (100 μM) in PBS buffer. (c) Time-scan of **NNP** upon addition with $ONOO^-$ (100 μM) in PBS buffer at 37 °C. Inset: The visual colors of probe **NNP** (50 μM) in the absence and presence of ONOO- (500 μM). (d) Fluorescence intensity of **NNP** at 560 nm upon addition with $ONOO^-$ (100 μM) in PBS buffer. (e) The linear ship between the fluorescence intensity of **NNP** at 560 nm and the concentration of $ONOO^-$. (f) Fluorescence intensity of NNP at 560 nm upon addition with varies analytes (100 μM) in PBS buffer. Numbers 1–24 represent: 1. ·OH; 2. $^1O_2$; 3. NO; 4. O^{2-};5. ClO; 6. H_2O_2; 7. Ac^-; 8. Cl^-; 9. CO_3^{2-}; 10. NO_2^-; 11. NO_3^-; 12. SO_3^{2-}; 13. S^{2-}; 14. Ca^{2+}; 15. K^+; 16. Na^+; 17. Mg^{2+}; 18. Fe^{2+}; 19. Al^{3+}; 20. Cu^{2+}; 21.GSH; 22. Cys; 23. Hcy; 24. $ONOO^-$. All spectra were monitored 5 min after mixing in PBS buffer (10 mM, pH 7.4, with 1% DMSO, CTAB 2 mM) at 37 °C. $\lambda_{ex} = 432$ nm, slit width: $d_{ex} = d_{em} = 10$ nm. (For interpretation of the references to color in this figure legend, the reader is referred to the Web version of this article.)

400 mg/kg NAC for 1.0 h, and then 400 mg/kg APAP (i.p.) for another 1.0 h. Balb/c nude mice were treated with 150 μL 50% EtOH solution by oral gavage and pretreated with or without 200 mg/kg APAP by intraperitoneal injection. In vivo mapping of the liver to model mice. Fluorescent images of mice were captured at different time interval within 3 h. The excited wavelength was set at 440 nm.

2.10. Pathological examination of liver tissue

The fixed liver tissue (contain wide-type group and model group) will be entrusted to the company (Wuhan Seville Biological Co., Ltd.) to cut into blank paraffin tissue sections of 4 μm for histopathological analysis. Thin sections (4 μm) were stained with Siriu Red, and Masson for histopathological study. Sirius Red and Masson-stained areas from 6 random fields were monitored by microscopy (Olympus IX73).

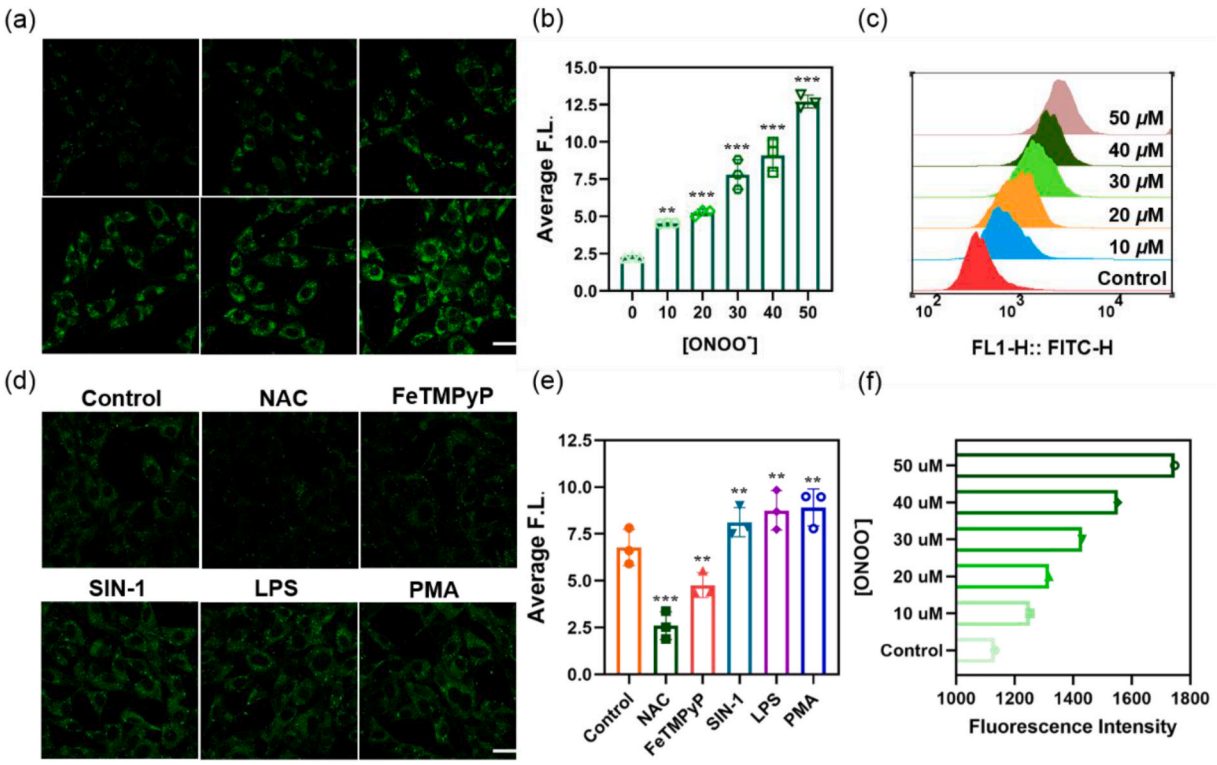

Fig. 4. Microscopy images of exogenous $ONOO^-$ in LX-2 cells. (a) The cells were stained with 10 μM **NNP** for 30 min and washed with DPBS for three times, and then pretreated with different concentration of $ONOO^-$ (0–50 μM) for 30 min. (b) Quantification of imaging data (a), n = 3, error bars were ±SD. (c) Flow cytometry assays of **NNP** activation by $ONOO^-$ (LX-2) cancer cells. Assays were performed by counting 10,000 cells that had been exposed to 10 μM probe for 30 min. (d) LX-2 cells were pretreated with or without NAC (1×10^{-3} M, 12 h), FeTMpyp (100×10^{-6} M, 0.5 h), SIN-1 (200×10^{-6} M, 0.5 h), LPS (0.1 μg mL^{-1}, 12 h), PMA (100×10^{-6} M, 1 h). Imaging after incubation with NNP (10 μM) for another 30 min. NAC(*N*-acetylcysteine) is the $ONOO^-$ scavenger, FeTMPyP is an $ONOO^-$ deconstruction reagent, SIN-1 is a potent vasorelaxant and inhibitor of platelet aggregation, also is an exogenous $ONOO^-$ donor, PMA (phorbol-12-myristate-13-acetate) is an $ONOO^-$ activator. (e) Quantification of imaging data (d), n = 3, error bars were ±SD. The images were obtained by collecting emissions at 530–600 nm nm upon excitation at 405 nm. Scale bar: 25 μm. (f) Quantification of flow cytometry data at median. *p-value < 0.05, **p-value < 0.01, ***p-value < 0.001.

After two groups of blank slices were treated by de-waxing, and staining with probe **NNP** for further divided by fluorescence intensity. The pre-treated slices were washed with PBS buffer for 3 times, and 5 min each time. Then the liver biopsy were stained with **NNP** (10 μM) for 30 min, and washed with PBS buffer for three times. After treated with DAPI for another 30 min. After sealing, images detected by a Lecia Two-photon fluorescence microscope equipped with 20× objective lens. The excited wavelength was set at 405 nm, and emission wavelengths were collected from 530 nm to 600 nm.

3. Results and discussion

3.1. Synthesis of the probe *NNP*

The synthesis approach of the probe **NNP** was illustrated in Fig. 2. The structure was confirmed by satisfactory spectroscopic data including ^{1}H NMR, ^{13}C NMR and HRMS (Figs. S1–S9 in Supplement Materials).

3.2. Optical properties of the probe *NNP*

Initially, the absorbance spectra of the probe **NNP** with and without $ONOO^-$ were scanned (Fig. 3a). The probe **NNP** itself showed a peak at 505 nm, whereas the mixture of **NPP** and $ONOO^-$ indicated two obvious peaks at 299 nm and 459 nm. This result inferred the significant response of **NNP** towards $ONOO^-$. Accordingly, under the excitation at 432 nm, the fluorescence spectrum of the probe **NNP** suggested no obvious peaks, whereas the mixture of **NPP** and $ONOO^-$ exhibited a remarkable fluorescence signal at 560 nm, which was a typical "turn-on" probe (Fig. 3b). Therefore the parameters were basically set (λ_{ex} = 432 nm, slit width: $d_{ex} = d_{em}$ = 10 nm, voltage = 600 V, 37 °C). The fluorescence quantum yield (FQY) of **NNP** was determined as 0.27 via the reference method. To check the working conditions, we subsequently involved the factors including pH and incubation time. As shown in Fig. S10, **NNP** itself kept stable in the pH range of 4–11, whereas the detecting system indicated steady fluorescence intensity in the range of 4–10. Such wide pH ranges ensured the application of the probe. Meanwhile, in Fig. 3c, we could see that the response completed within 25 s, accompanied by the color change from red to yellow. That was to say, **NNP** inferred a rapid response towards $ONOO^-$, which was beneficial for detecting such a transient target. As for the stability, both **NNP** itself and the detection system could retain unchanged after 48 h (Fig. S11).

In Fig. 3d, when the concentration of $ONOO^-$ increased from 0 to 100 μM (10 equiv.), the fluorescence of the detection system indicated an enhancement accordingly. The plateau could be reached at about 50 μM (5 equiv.) (Fig. S12). According to the linear correlation (Fig. 3e), **NNP** could monitor $ONOO^-$ linearly in the range of 0–10 μM (0–1 equiv.). Further, the Limit of Detection (LOD) was calculated as 0.13 μM. The results above suggested that **NNP** could realize the quantitative detection of $ONOO^-$ with high sensitivity.

One step further, the selectivity of **NNP** for $ONOO^-$ from other analytes was evaluated. As shown in Fig. 3f, only $ONOO^-$ could cause the obvious fluorescence enhancement. Other analytes, no matter common ions, anions or ROS, caused no notable variation in fluorescence intensity. In the coexistence systems containing $ONOO^-$ and other analytes, the fluorescence response to $ONOO^-$ seemed not interfered, except for the reductive species such as SO_3^{2-}, S^{2-} and so on (Fig. S13).

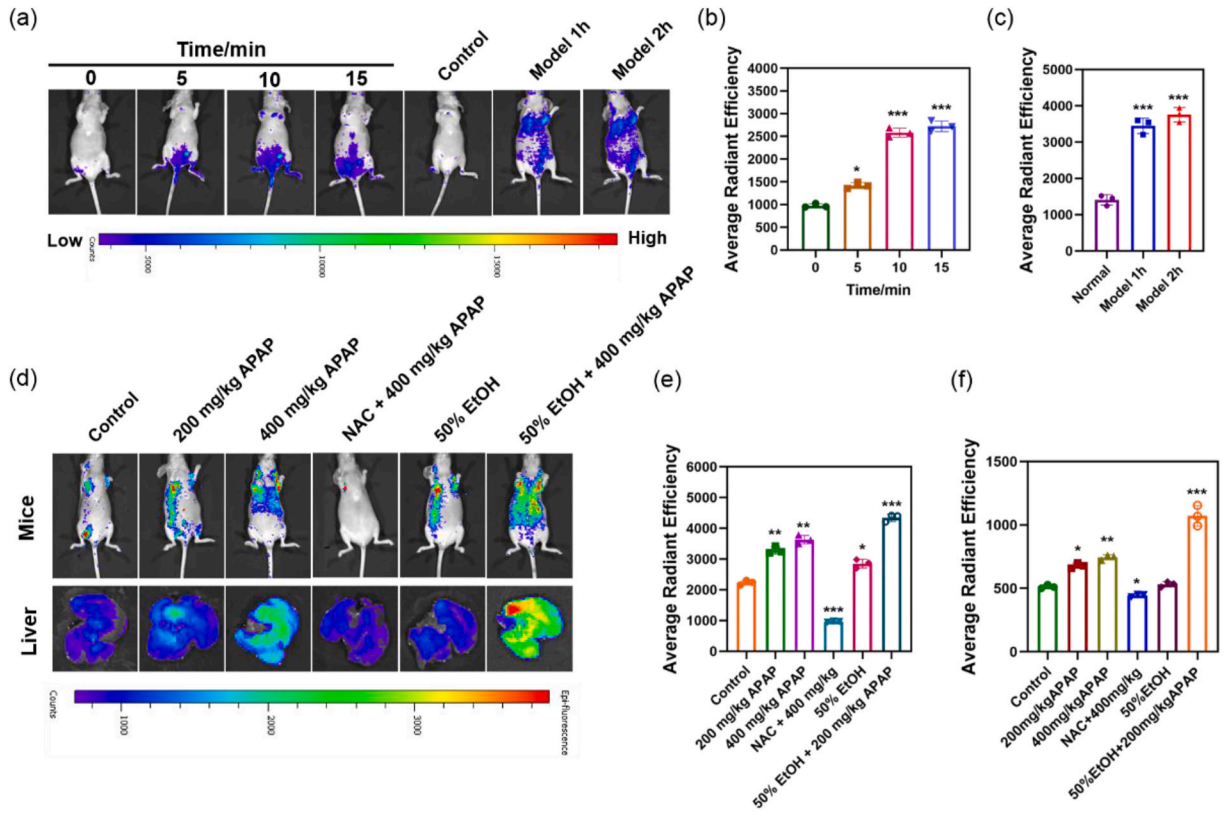

Fig. 5. (a) *In vivo* fluorescence imaging of BALB/c mice. The mice were intraperitoneal injected with 200 μL of probe (100 μM in saline) and then injected 400 μL $ONOO^-$ solution (500 μM in saline) was the time-course imaging at 0, 5 10, 15 min. *In vivo* mapping of $ONOO^-$ deposition in ALI model mice. Comparison of the fluorescent image at 60 min after intravenous injection of 100 μM of **NNP** into wild-type mice and ALI mice. (b) Quantification of imaging data from (a). (c) Quantification of imaging data from (a). (d) *In vivo* mapping of APAP-induced liver injury model mice. Balb/c nude mice were administrated (i.p.) with 0 mg/kg, 200 mg/kg, 400 mg/kg APAP for 1.0 h. Babl/c nude mice were first administrated (i.p.) with 400 mg/kg NAC for 1.0 h, and then 400 mg/kg APAP (i.p.) for another 1.0 h. Balb/c nude mice were treated with 150 μL 50% EtOH solution by oral gavage and pretreated with or without 200 mg/kg APAP by intraperitoneal injection. In vivo mapping of the liver to model mice after intravenous injection of 100 μM of NNP into mice. (e) Quantification of imaging data from image of model mice. (f) Quantification of imaging data from image of liver. n = 3, error bars were ±SD. Statistical analysis was performed with a two-tailed Student's *t*-test with unequal variance, *p value < 0.05, **p value < 0.001, ***p value < 0.001.

Anyway, in real cases, the selectivity of **NNP** could be maintained basically.

3.3. Intracellular imaging

Since the research object was ALI, in the intracellular experiments, we used LX-2 cells (Human hepatic stellate cell line). Before the application in cellular imaging, the cell cytotoxicity was assessed with a standard CCK-8 method (Fig. S14). After the treatment with 40 μM of **NNP** for 24 h, the survival rate of LX-2 cells was still over 80%. Subsequently, we attempt to check the correlation between the fluorescence signals and the concentration of $ONOO^-$ in living cells. In Fig. 4a&b, the **NNP** concentration was set as 10 μM while the incubation time was set as 30 min for insurance. The fluorescence signals showed a dose-dependent enhancement with various concentrations of $ONOO^-$ (0–50 μM). Commonly, Chlorine-related metabolites were nonnegligible interferences in detecting $ONOO^-$. In Fig. S15, we checked the response of our probe towards ClO^- and ClO_4^-. The results showed that **NNP** could exclude the interferences from these metabolites. Moreover, in the flow cytometry analysis, the result agreed with that on confocal imaging (Fig. 4c&f). As one notable point, the intracellular microenvironment in living cells was quite different from the PBS buffer, thus the incubation process should be evaluated for a second time. Besides, in Fig. S16, the buffer containing 1% DMSO and 0.1% DMSO were compared, these two buffer systems did not show obvious difference in fluorescence intensity during the imaging of exogenous $ONOO^-$ in LX-2 cells. In Fig. S17, when incubated with $ONOO^-$ (50 μM), the fluorescence of **NNP** (10 μM) exhibited gradually stronger fluorescence intensity along with the increase of incubation time from 0 to 30 min. Although the incubation time was prolonged, the detection of $ONOO^-$ was relatively stable, which inferred that **NNP** could work well in cellular microenvironment when the incubation time was set as 30 min. Therefore in the *in vivo* experiment, we consulted this result as a referable parameter. Further, in Fig. 4d&e, in the LX-2 cells treated with NAC(*N*-acetylcysteine, the $ONOO^-$ scavenger), FeTMPyP (an $ONOO^-$ deconstruction reagent), SIN-1 (a potent vasorelaxant and inhibitor of platelet aggregation, also an exogenous $ONOO^-$ donor) and PMA (phorbol-12-myristate-13-acetate, an $ONOO^-$ activator), the fluorescence intensity varied correspondingly. Accordingly, the regulated $ONOO^-$ level could be reflected by the fluorescence intensity by using our probe **NNP**.

3.4. In vivo application in mice acute liver injury model

Upon the results in Human hepatic stellate cell line, we further constructed the ALI model in BALB/c mice to evaluate the performances of the probe **NNP**. Two independent models were checked. The acute liver injury in this work was initially induced by CCl_4/olive oil via intraperitoneal injection. Then the *in vivo* fluorescence imaging of BALB/c mice was performed and the results were exhibited in Fig. 5. As shown in Fig. 5a and b, in normal mice, the pre-injected probe **NNP** (100 μM in saline) could response to the injected $ONOO^-$ (500 μM in saline) in a time-dependent manner. As the incubation time prolonged,

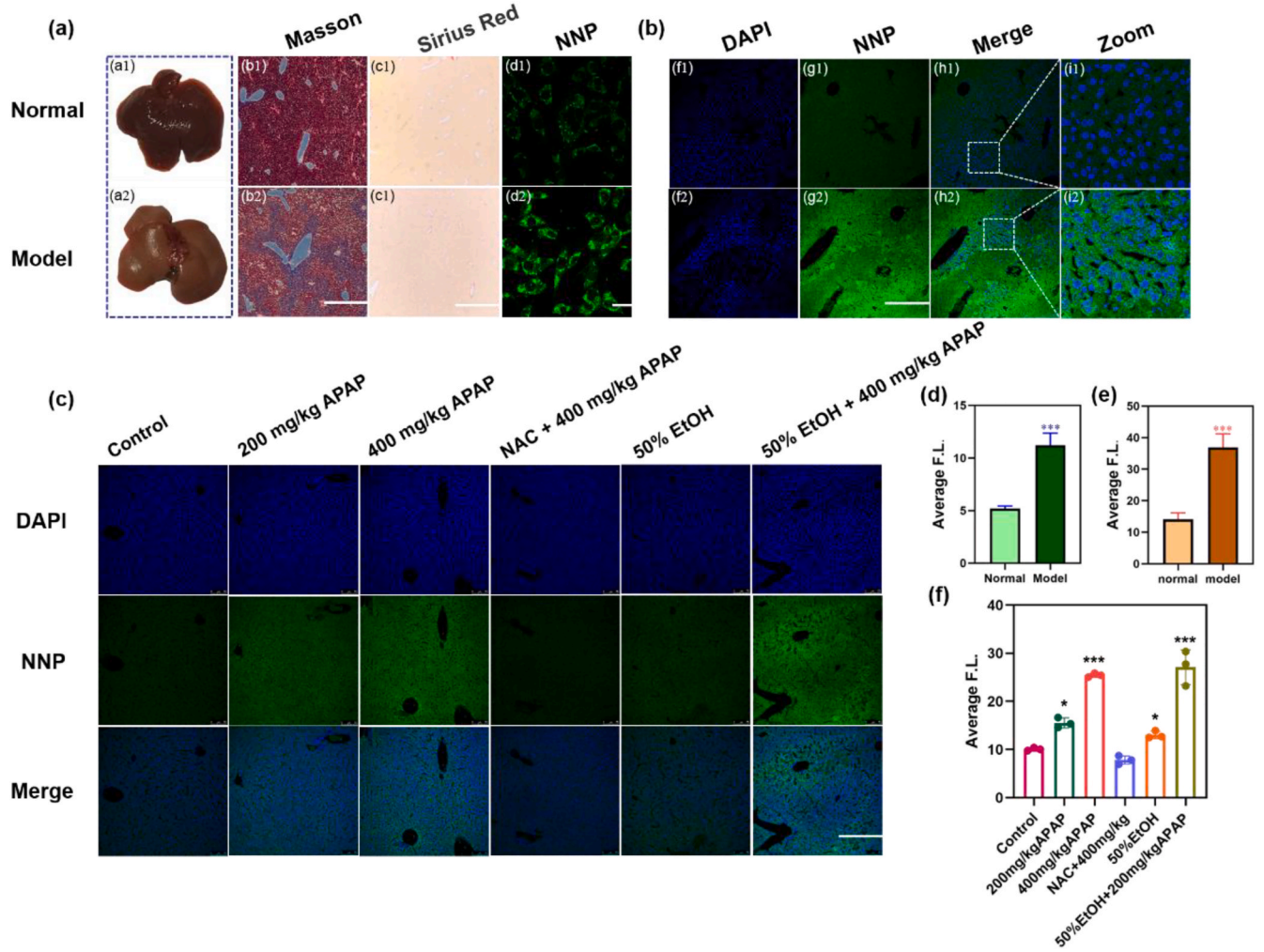

Fig. 6. (a) Livers, normal liver, ALI model liver. Immunohistological analysis with Masson and Sirius red, normal liver, ALI model liver. Scale bars: 50 μm. Microscopy images of endogenous $ONOO^-$ in LX-2 cells. The cells were treated with PBS and 1 mM CCl_4 for 4 h. Then the cells were stained with 10 μM **NNP** for 30 min. Scale bar: 25 μm. (b) Microscopy images of liver biopsy, normal liver biopsy, ALI model liver biopsy. The liver biopsy were stained with **NNP** (10 μM) for 30 min, and then treated with DAPI for another 30 min. (c) Microscopy images of liver biopsy, the liver of Balb/c nude mice were administrated (i.p.) with 0 mg/kg, 200 mg/kg, 400 mg/kg APAP for 1.0 h. Babl/c nude mice were first administrated (i.p.) with 400 mg/kg NAC for 1.0 h, and then 400 mg/kg APAP (i.p.) for another 1.0 h. The liver of Balb/c nude mice were treated with 150 μL 50% EtOH solution by oral gavage and pretreated with or without 200 mg/kg APAP by intraperitoneal injection. The liver biopsy were stained with **NNP** (10 μM) for 30 min, and then treated with DAPI for another 30 min. (d) Quantification of imaging data (a). n = 3, error bars were ±SD. Statistical analysis was performed with a two-tailed Student's *t*-test with unequal variance, ***p value < 0.001. The images were obtained by collecting emissions at 530–600 nm upon excitation at 405 nm. Scale bar: 25 μm. (e) Quantification of imaging data (b). (f) Quantification of imaging data (c). n = 3, error bars were ±SD. Statistical analysis was performed with a two-tailed Student's *t*-test with unequal variance, *p value < 0.05, ***p value < 0.001. The images were obtained by collecting emissions at 530–600 nm upon excitation at 405 nm. Scale bar: 50 μm. (For interpretation of the references to color in this figure legend, the reader is referred to the Web version of this article.)

the fluorescence signals enhanced and reached the plateau within 15 min. Meanwhile, in the control group with wild-type mice, no obvious fluorescence signal could be observed in 2 h, whereas in the ALI group, a dramatic fluorescence enhancement could be observed, in both the pictures taken in 1 h and 2 h (Fig. 5a&c). A majority of the signals were around the liver region of the ALI mice.

To avoid the interference of elemental chlorine and hypochlorous acid, we built the acetaminophen (APAP)-induced hepatotoxicity model. In Fig. S18, the fluorescence signal in normal mice showed the peak value at 15 min and was then eliminated gradually. In Fig. 5 d-f, the fluorescence intensity of the mice and the liver were measured. As a result, the probe **NNP** could reflect the dose-dependent accumulation of $ONOO^-$ by APAP and the elimination of $ONOO^-$ by NAC. Notably, 50% EtOH could induce the generation of $ONOO^-$, and this kind of injury could also be detected by our probe. The above results indicated that **NNP** could monitor the $ONOO^-$ level in the occurrence of ALI in situ with a steady performance.

The following experiments including histopathological, immunohistochemical and imaging studies were conducted by using a small portion of the liver tissues in the above imaging procedure. Initially, the serum liver injury indexes were tested by using corresponding ELISA kits (Fig. S15). The tested indexes included ALT (Alanine aminotransferase), AKP (Alkaline phosphatase), LDH (Lactate dehydrogenase), TBIL (Total bilirubin), IV-C (Collage Type IV) and HYP (Hydroxyproline). All the tested indexes were much higher in the ALI model liver than in the control, which inferred that the model group was suffering ALI in diagnostics. Afterwards, the immunohistological analysis of the liver tissues were performed by using Masson and Sirius red staining (Fig. 6a–c). In appearance, the normal liver tissue (Fig. 6a1) was in dark red with luster, whereas the ALI model liver tissue (Fig. 6a2) was pale. After Masson staining, the normal group was in bright rose red (Fig. 6b1), whereas the ALI group exhibited the blue patches due to the progress of

fibrosis (Fig. 6b2). Meanwhile, after Sirius red staining, the normal group indicated yellowish red color (Fig. 6c1), whereas the ALI group with fibrosis showed faint yellow color (Fig. 6c2). Besides, we used CCl_4 to induce the ALI event in LX-2 cells, and the endogenous $ONOO^-$ was then detected by the probe NNP (10 μM). In the control group, the green fluorescence was weak (Fig. 6d1), which indicated the low endogenous $ONOO^-$ level in living LX-2 cells. Remarkably, in the induced ALI group, the green fluorescence was much stronger (Fig. 6d2), which inferred the high endogenous $ONOO^-$ level due to ALI. The quantification analysis from the imaging results also convinced the significant increase of endogenous $ONOO^-$ level (Fig. 6e). Furthermore, the liver biopsy was conducted under fluorescent microscopy. The general position of the nucleus was labeled by DAPI (Fig. 6f1, f2). In the green channel, it was easy to conclude that low $ONOO^-$ concentration in control (Fig. 6g1) and high $ONOO^-$ concentration in the ALI liver tissue (Fig. 6g2) could be significantly distinguished by **NNP** through the comparison the fluorescence intensity. The merged pictures (Fig. 6h1, h2), the zoomed images (Fig. 6i1, i2) and the quantification analysis (Fig. 6d&e) all confirmed the capability of **NNP** for the detection of endogenous $ONOO^-$ in ALI liver tissues. The similar analysis was conducted on the liver tissues of the APAP-induced ALI model (Fig. 6c&f). Both the visual pictures and the quantification of imaging data agreed with the results of the *in vivo* imaging above.

4. Conclusion

To sum up, we developed a novel fluorescent probe, **NNP**, for the detection of $ONOO^-$ in acute liver injury. Under the excitation at 432 nm, **NNP** could response to $ONOO^-$ with a remarkable fluorescence enhancement at 560 nm. The fluorescence quantum yield of **NNP** was determined as 0.27. The *in vitro* evaluation of **NNP** indicated the advantages including high sensitivity (LOD = 0.13 μM), rapid response (<25 s), naked-eye (red to yellow), and stability under various pH (4–10) and time (>48 h) conditions. In Human hepatic stellate LX-2 cells, **NNP** could realize the dose-dependent detection of $ONOO^-$, while the cytotoxicity was relatively low. In the ALI model mice, **NNP** could monitor the $ONOO^-$ level in the occurrence of ALI in situ with a steady performance. A majority of the signals were around the liver region of the ALI mice, and the fluorescence intensity generated in 1 h did not show obvious decay in 2 h. Further immunohistochemical and imaging studies confirmed the diagnostic characteristics of the constructed ALI model as well as the imaging capability of **NNP** in the liver tissues. As a result, **NNP** could achieve the detection of endogenous $ONOO^-$ in ALI liver tissues. More than introducing a practical implement for the $ONOO^-$ detection in ALI, this work provided a referable example for the establishment of molecular indexes in pre-clinical diagnosis.

Declaration of competing interest

There is no conflict of interest to declare.

Acknowledgments

This research was supported by grants of Postdoctoral Science Foundation of China (No. 2019M651781 and 2019TQ0142).

Appendix A. Supplementary data

Supplementary data to this article can be found online at https://doi.org/10.1016/j.redox.2021.102068.

References

[1] R. Taub, R. Taub, Liver regeneration: from myth to mechanism, Nat. Rev. Mol. Cell Biol. 5 (2004) 836–847. Nature Reviews Molecular Cell Biology 5(10).
[2] O. Osborn, J.M. Olefsky, The cellular and signaling networks linking the immune system and metabolism in disease, Nat. Med. 18 (3) (2012) 363–374.
[3] T.C. Li, M.R. Versland, G.Y. Wu, Drug-Induced Hepatotoxicity, Diseases of the Liver and Bile Ducts 1998.
[4] J.D. Browning, J.D. Horton, Molecular mediators of hepatic steatosis and liver injury, J. Clin. Invest. 114 (2) (2004) 147–152.
[5] S.K. Asrani, H. Devarbhavi, J. Eaton, P.S. Kamath, Burden of liver diseases in the world, J. Hepatol. 70 (1) (2019) 151–171.
[6] W. Bernal, J. Wendon, Acute liver failure, N. Engl. J. Med. 369 (26) (2013) 2525–2534.
[7] M. Mosedale, P.B. Watkins, Drug-induced liver injury: advances in mechanistic understanding that will inform risk management, Clin. Pharmacol. Therapeut. 101 (4) (2017).
[8] P. Zhang, H. Wang, Y. Hong, M. Yu, R. Zeng, Y. Long, J. Chen, Selective visualization of endogenous hypochlorous acid in zebrafish during lipopolysaccharide-induced acute liver injury using a polymer micelles-based ratiometric fluorescent probe, Biosens. Bioelectron. 99 (2017) 318–324.
[9] R.J. Church, G.A. Kullak-Ublick, J. Aubrecht, H.L. Bonkovsky, N. Chalasani, R. J. Fontana, J.C. Goepfert, F. Hackman, N. King, S. Kirby, Candidate biomarkers for the diagnosis and prognosis of drug-induced liver injury: an international collaborative effort, Hepatology 69 (2018) 760–773.
[10] Daniele Prati, Emanuela Taioli, Alberto Zanella, Torre Della, Sonia Butelli, Updated definitions of healthy ranges for serum alanine aminotransferase levels, Ann. Intern. Med. 137 (2002) 1–9.
[11] M. Panteghini, Aspartate aminotransferase isoenzymes, Clin. Biochem. 23 (4) (1990) 311–319.
[12] M. Plebani, ., R. Gava, . [Alkaline Phosphatase], Alkaline Phosphatase 1979.
[13] E. Schmidt, F. Schmidt, γ-Glutamyltranspeptidase, Methods Enzymol. 77 (34) (1973) 237–253.
[14] Advantages of glutamate dehydrogenase as a blood biomarker of acute hepatic injury in rats, Lab. Anim. 36 (3) (2002) 313–321.
[15] Circulating microRNAs as potential markers of human drug-induced liver injury, Hepatology 54 (5) (2011).
[16] H. Ko Ba Yashi, M. Ogawa, R. Alford, P.L. Choyke, Y. Urano, New strategies for fluorescent probe design in medical diagnostic imaging, Chem. Rev. 110 (5) (2010) 2620–2640.
[17] D. Wu, A.C. Sedgwick, T. Gunnlaugsson, E.U. Akkaya, J. Yoon, T.D. James, Fluorescent chemosensors: the past, present and future, Chem. Soc. Rev. 46 (2017).
[18] H. Jaeschke, Reactive oxygen and mechanisms of inflammatory liver injury: present concepts, J. Gastroenterol. Hepatol. 26 (2011).
[19] A. Wiseman, Dietary alkyl thiol free radicals (RSS) can be as toxic as reactive oxygen species (ROS), Med. Hypotheses 63 (4) (2004) 667–670.
[20] X. He, L. Li, F. Yu, S. Wen, X. Li, H. Ma, In vivo imaging of leucine aminopeptidase activity in drug-induced liver injury and liver cancer via a near-infrared fluorescent probe, Chem. Sci. 8 (2017).
[21] T. Obata, M. Aomine, Changes in monoamine oxidase activity in hepatic injury: a review, Res. Commun. Mol. Pathol. Pharmacol. 122–123 (1–6) (2014) 51–63.
[22] N.J. Fernandez, B.A. Kidney, Alkaline phosphatase: beyond the liver, Vet. Clin. Pathol. 36 (2007) 223–233.
[23] G. Ferrer-Sueta, N. Campolo, M. Trujillo, S. Bartesaghi, S. Carballal, N. Romero, B. Alvarez, R.R. AdI, Biochemistry of peroxynitrite and protein tyrosine nitration, Chem. Rev. 118 (2018) 1338–1408, acs.chemrev.7b00568.
[24] S.B.A. B, R.R.A. B, Fundamentals on the biochemistry of peroxynitrite and protein tyrosine nitration, Redox Biol. 14 (2018) 618–625.
[25] P. Pacher, J.S. Beckman, L. Liaudet, Nitric oxide and peroxynitrite in Health and disease, Physiol. Rev. 87 (1) (2007) 315–424.
[26] R. Radi, Oxygen radicals, nitric oxide, and peroxynitrite: redox pathways in molecular medicine, Proc. Natl. Acad. Sci. Unit. States Am. 115 (23) (2018) 201804932.
[27] W. Shu, Y. Wu, S. Zang, S. Su, X. Zhang, A mitochondria-targeting highly specific fluorescent probe for fast sensing of endogenous peroxynitrite in living cells, Sensor. Actuator. B Chem. 303 (2019) 127284.
[28] D. Wang, Y. Huyan, X. Nan, H. Li, Y. Xu, Product-boosted fluorescence signal: a new approach for designing small-molecule probes for detection of peroxynitrite, Chem. Commun. 56 (57) (2020).
[29] Y. Zuo, X. Wang, W. Lin, Four-armed functional siloxane enables ratiometric unconventional fluorescence for the detection of ONOO - ScienceDirect, Sensor. Actuator. B Chem. 331 (2021) 129462.
[30] Y. Deng, G. Feng, Visualization of ONOO – and viscosity in drug-induced hepatotoxicity with different fluorescence signals by a sensitive fluorescent probe, Anal. Chem. 92 (21) (2020) 14667–14675.
[31] Time-resolved luminescence detection of peroxynitrite using a reactivity-based lanthanide probe, Chem. Sci. 11 (2020).
[32] W. Wang, C. Wang, C. Zhong, Z. Liu, Visualizing peroxynitrite in microvessels of the brain with stroke using an engineered highly specific fluorescent probe, ACS Sens. 5 (2020) 3237–3245.
[33] X. Zhang, Y. Chen, C. Liu, Z. Zhuang, W. Sheng, A novel hexahydropyridazin-modified rhodamine fluorescent probe for tracing endogenous/exogenous peroxynitrite in live cells and zebrafish, Dyes Pigments 170 (2019) 107573.
[34] Imaging of peroxynitrite in drug-induced acute kidney injury with a near-infrared fluorescence and photoacoustic dual-modal molecular probe, Chem. Commun. 56 (2020).
[35] W.L. Jiang, Y. Li, W.X. Wang, Y.T. Zhao, J. Fei, C.Y. Li, A hepatocyte-targeting near-infrared ratiometric fluorescent probe for monitoring peroxynitrite during drug-induced hepatotoxicity and its remediation, Chem. Commun. 55 (95) (2019) 14307–14310.
[36] D. Cheng, X. Gong, Q. Wu, J. Yuan, X.B. Zhang, High-selectivity fluorescent reporter toward peroxynitrite in a coexisting nonalcoholic fatty liver and drug-

induced liver diseases model, Anal. Chem. 92 (16) (2020) 11396–11404. XXXX (XXX).
[37] G. Jiang, C. Li, Q. Lai, X. Liu, B.Z. Tang, An easily available ratiometric AIE probe for peroxynitrite in vitro and in vivo imaging, Sensor. Actuator. B Chem. 329 (2021) 129223.
[38] Indication of dynamic peroxynitrite fluctuations in the rat epilepsy model with a near-infrared two-photon fluorescent probe, Anal. Chem. 93 (4) (2021).
[39] X. Yin, W. Feng, S. Gong, G. Feng, Near-infrared fluorescent probe with rapid response and large Stokes shift for imaging peroxynitrite in living cells, zebrafish and mice, Dyes Pigments 172 (2019) 107820.
[40] D. Cheng, W. Xu, X. Gong, L. Yuan, X.B. Zhang, Design strategy of fluorescent probes for live drug-induced acute liver injury imaging, Acc. Chem. Res. 54 (2) (2020).
[41] L. Yuan, W. Lin, S. Zhao, W. Gao, B. Chen, L. He, S. Zhu, A unique approach to development of near-infrared fluorescent sensors for in vivo imaging, J. Am. Chem. Soc. 134 (32) (2012) 13510–13523.
[42] Z. Li, Imaging of hydrogen peroxide (H2O2) during the ferroptosis process in living cancer cells with a practical fluorescence probe, Talanta 212 (2020) 120804.